Active thermography inspection of surface-whitened mortars – measurement of surface spectral absorptivity for investigation of efficient heating light wavelengths

Masashi Ishikawa[a*], Akira Emoto[b], Yoshihiro Suto[a], Hideo Nishino[a]

[a] *Graduate School of Technology, Industrial and Social Sciences, Tokushima University, 2-1 Minamijosanjima, Tokushima, 770-8506, Japan*

[b] *Institute of Post-LED Photonics, Tokushima University, 2-1 Minamijosanjhma, Tokushima 770-8506, Japan*

*Corresponding author. Email: m.ishikawa@tokushima-u.ac.jp

Abstract

The surface spectral absorptivity of surface-whitened mortars due to the occurrence of efflorescence (i.e., mortars whose surface was covered with calcium carbonate) was measured, and the relationship between the spectral absorptivity and inspection capability of active thermography inspection was investigated. The spectral absorptivity of mortars increased significantly at a wavelength of approximately 3000 nm regardless of the presence/absence of the discoloration. Experiments for mortar specimens using optical lights with wavelengths in the visible, short wavelength, and medium/long wavelength ranges showed that the heating efficiency and defect detection capability of active thermography inspection were correlated with the surface spectral absorptivity, and were higher when long wavelength light was used as a heater. Defects in the surface-whitened mortar specimen were detected more efficiently when the specimen was heated using a CO_2 laser, whose wavelength is in the long wavelength range, than when using an optical light having a wavelength in the visible/short wavelength range.

Keywords

Non-destructive inspection; Infrared thermography; Spectral measurement; Concrete; Efflorescence

1. Introduction

Infrared active thermography is a promising non-destructive inspection method. In this method, an inspection object is artificially heated, and the surface temperature during or after heating is observed using an infrared camera. For heating the inspection object, various methods, such as using optical lamps [1–4], air heaters [5, 6], laser heating [7–9], ultrasound [10–12], eddy current [13–15], etc., have been reported in many works. Among these methods, surface heating using optical lamps is one of frequently used methods for the inspection of structural components or for laboratory tests. When there is a defect in the object (e.g., a crack or delamination), the heat flow from the surface is disturbed by the defect, causing a local temperature irregularity around the defect. The defect is then identified by detecting the temperature abnormality in the thermal image obtained using the infrared camera. This method is non-contact and can easily inspect a wide area; thus, it is used for the inspection of various objects, including civil structures [16–19], mechanical components [20–23], composite materials [24–27], and additive manufactured components [28, 29]. However, the observed temperature is easily affected by the spectral characteristics of the inspected object surface, which can also affect the inspection results. For example, when inspecting concrete structures, the discoloration of the concrete surface can be an obstacle to thermographic inspection. Concrete surfaces can be blackened or whitened depending on those conditions. Surface blackening is caused in a polluted (or dusty) environment or by the growth of black crust. Surface whitening, on the other hand, is mainly caused by the occurrence of efflorescence [30, 31]. Efflorescence is the deposition of salts migrated from the interior of the mortar; in many cases, its major components is calcium carbonate caused by the reaction of calcium hydroxide in the mortar with carbon dioxide in the air. The occurrence of efflorescence can be a greater obstacle in active thermography inspections than the surface blacking; because it is a white deposit, visible and near-visible light should reduce absorptivity. The reduction of the absorptivity leads to the reduction of the input heat in active thermography, resulting in the deterioration of its inspection capability [32, 33].

This study focuses on the inspection of surface-whitened mortars and investigates the relationship between the surface spectral absorptivity and the inspection capability of active thermography inspection. First, the spectral absorptivity of whitened mortar specimens simulating the discoloration caused by efflorescence was measured using spectrometers. Subsequently, to verify the measured spectral absorptivity, the specimens were heated using optical lights with different wavelengths, and the heating efficiencies caused by the different lights were compared.

Finally, mortar specimens with an artificial defect were inspected by active thermography using an optical lamp or laser, and the relationship between the wavelength of the incident light and defect detection capability was examined. From the obtained results, the wavelengths of heating light efficient for active thermography inspection of discolored mortars were investigated.

2. Measurement of surface spectral absorptivity

Spectral measurements were performed to investigate the spectral absorptivity of incident light into mortars.

2.1 Specimens and measurements

Three mortar specimens (named S_{norm}, S_{CaCO3}, and S_{black}) were prepared. S_{norm} is a normal mortar specimen without discoloration (Fig. 1(a)). In contrast, the surface of S_{CaCO3} is covered with calcium carbonate, simulating the occurrence of efflorescence (Fig. 1(b)); the specimen was prepared by pouring calcium carbonate aqueous solution over the mortar surface and drying it at room temperature. The S_{black} is a specimen prepared as a reference (Fig. 1(c)), and its surface was coated with black-body paint (TA410KS, ICHINEN TASCO Co., LTD.). Each specimen was 38 mm and 5.6 mm in diameter and thick, respectively. The surface spectral absorptivity of these specimens was measured in the visible (400–900 nm), short wavelength (1350–2500 nm), and medium/long wavelength (2500–12000 nm) ranges (note that the division of the infrared bands in this study was determined by referencing the manual book of the infrared camera used in the following experiments [34]). The spectrometers for the measurement of the visible, short, and medium/long wavelength ranges were FLAME-S-UV-VIS-ES (Ocean Insight Inc.), NeoSpectra-Micro (Si-Ware Systems Inc.), and FT-IR 680-IR (Agilent Technologies Inc.), respectively. All the measurements were performed using the diffuse reflectance method (basically similar to diffuse geometry, specular component included (8:di) [35]). Subsequently, the measured spectral absorptivity of S_{norm} and S_{CaCO3} were normalized by that of S_{black} to obtain the relative absorptivities (A_r) of S_{norm} and S_{CaCO3} assuming the spectral absorptivity of the S_{black} as 100%.

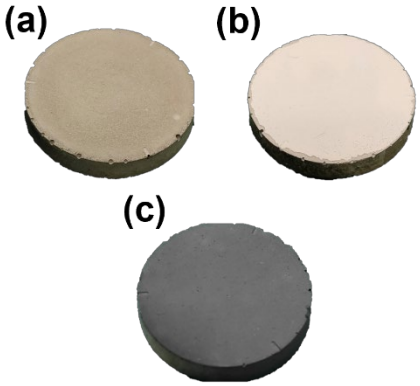

Fig. 1 Mortar specimens used for measurement of spectral absorptivity: (a) S_{norm}, (b) S_{CaCO3}, and (c) S_{black}.

2.2 Measurement results

The measured relative absorptivities A_r of the S_{norm} and S_{CaCO3} specimens are presented in Fig. 2 (the vertical axis in Fig. 2 indicates A_r). The absorptivity of the S_{norm} and S_{CaCO3} specimens in the visible and short wavelength ranges were approximately 70% and 20%, respectively. The absorptivity of S_{CaCO3}, which simulates the discoloration caused by efflorescence, was significantly smaller than that of S_{norm}. This means that using light in the visible/short wavelength range is inefficient for the active thermography inspection of surface-whitened mortars. In contrast, the absorptivity of both specimens increased at a wavelength of approximately 3000 nm. The average absorptivity of S_{norm} in the wavelength range greater than 8000 nm was approximately 100%, and that of S_{CaCO3} was 70–80%. This indicates that long wavelength light is suitable for the inspection of mortars, including discolored mortar.

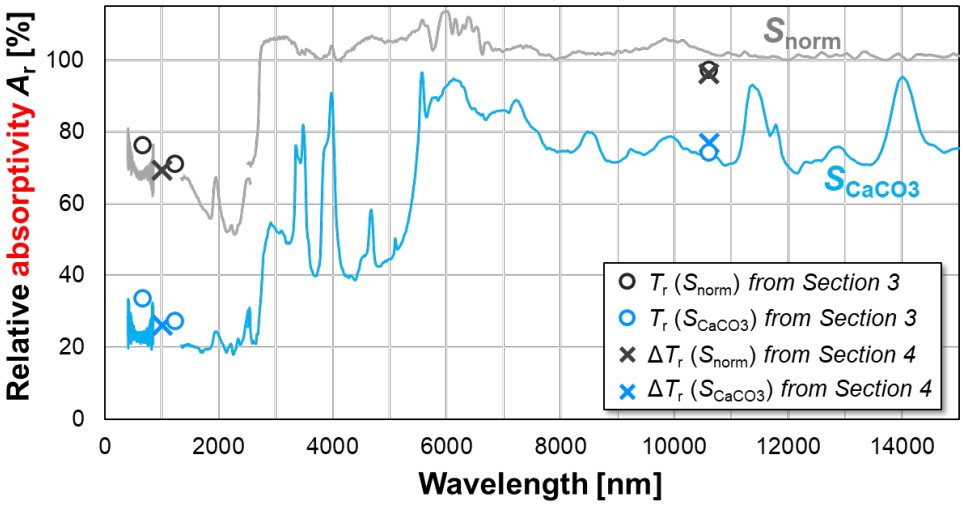

Fig. 2 Relationship between surface absorptivity A_r of S_{norm} and S_{CaCO3} specimen and wavelength

of incident light (solid lines). Circle and cross plots represent the results of the experiments in Sections 3 and 4, respectively.

3. Relationship between heating efficiency and wavelength of heating light

The specimens presented in Fig. 1 were heated using three different wavelength ranges (visible, short, and medium/long wavelength ranges), and the difference in heating efficiency caused by the different wavelength lights was compared with the results of the surface spectral absorptivity.

3.1 Experimental setup

Figure 3(a) shows the experimental setup using visible light, which was heated using a 500 W halogen lamp with an optical short-pass filter (< 900 nm, HA50, HOYA Co., Ltd.). Halogen lamps emit light in a broadband wavelength range from visible to approximately 3,500 nm [36]. Thus, by filtering the light from the halogen lamp, only visible light is selectively emitted. For the experiment in the short wavelength range, two filters (short-pass filter; SP-1600, IR-System Co., Ltd., and long-pass filter; IR85N, HOYA Co., Ltd.) were placed between the specimen and the halogen lamp to limit the wavelength range to 850–1600 nm (Fig. 3(b)). Experiments in the long wavelength range were performed using 46 W CO_2 laser equipment (Multiscan VS, Rofin-Baasel, Inc.); the wavelength of the CO_2 laser was 10600 nm (Fig. 3(c)). The emitted laser beam had a focal point at the distance of 147 mm from the laser head and expanded as the heating distance becomes farther than the focal distance. In the experiment, the specimens were placed at approximately 1 m away from the laser head; at this distance, the expanded laser beam covered nearly whole surface of the specimens. The specimens were heated for 100 s using visible and short wavelength light. When a CO_2 laser was used, the specimens were heated for 1.6 s because the heating power of the CO_2 laser was much larger than that of visible/short wavelength light. In the experiments, the temperature increases in the non-heated surface (i.e., the rear surface, not the heated surface) of the specimens were observed using an infrared camera (A315, Teledyne FLIR LLC); the infrared camera was equipped with 320 × 240 uncooled microbolometer detectors with a detectable wavelength range of 7.5–13 μm. The distance between the specimen and camera was approximately 300 mm, and the observed back surface of the specimens was coated with black-body paint. The temperatures were observed not only during heating but also after heating. The

total observation times were 140 s and 60 s for visible/short wavelength light heating and CO_2 laser heating, respectively.

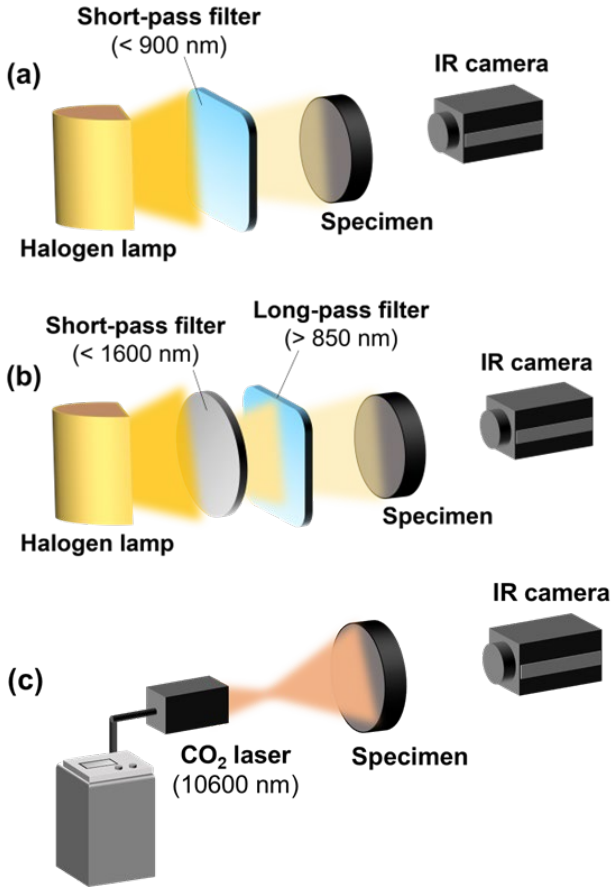

Fig. 3 Schematic of the experimental setup when specimens are heated using light with a wavelength of (a) visible, (b) short wavelength, and (c) long wavelength ranges.

3.2 Results

The temperature increases of the three specimens observed when each wavelength of light was used are presented in Fig. 4. It is worse noting that the temperatures obtained when using CO_2 laser (Fig. 4(c)) were similar to the temperature curves obtained when measuring thermal diffusivity using Parker's method [37] because the heating duration of laser heating was much shorter than that of halogen lamp heating. To compare the observed temperature increases with the spectral absorptivities presented in Fig. 2, the relative temperature increases (T_r) of S_{norm} and S_{CaCO3} were obtained by normalizing these temperatures by those of S_{black} (thus, in the T_r values, the influence of different output power due to the difference in the heating devices was cancelled, and only the effect of differences in the surface absorption properties was reflected). The obtained T_r values are presented in Fig. 5. In this figure, the scales on the horizontal axes agree with those

in Fig. 4; the noisy data observed immediately after the start of heating was caused by the small temperatures in early stage (see in Fig. 4). Figure 5 shows that T_r obtained when using the CO_2 laser is larger than that obtained when visible or short wavelength light is used. In addition, the difference between the T_r of S_{norm} and S_{CaCO3} (i.e., the reduction in T_r due to discoloration) is the smallest when using the CO_2 laser. These results show that long wavelength light is effective for heating mortars, including discolored mortars owing to efflorescence. T_r values in each wavelength range are presented in Fig. 2 as open circles. The plotted T_r values were determined as the average of the values for 110–140 s in Fig. 5(a) and (b) (visible and short wavelength ranges) and for 30–60 s in Fig. 5(c) (long wavelength range). These results indicate that T_r at each wavelength agrees with the spectral absorptivity A_r. This implies that the heating efficiency is correlated with the surface spectral absorptivity.

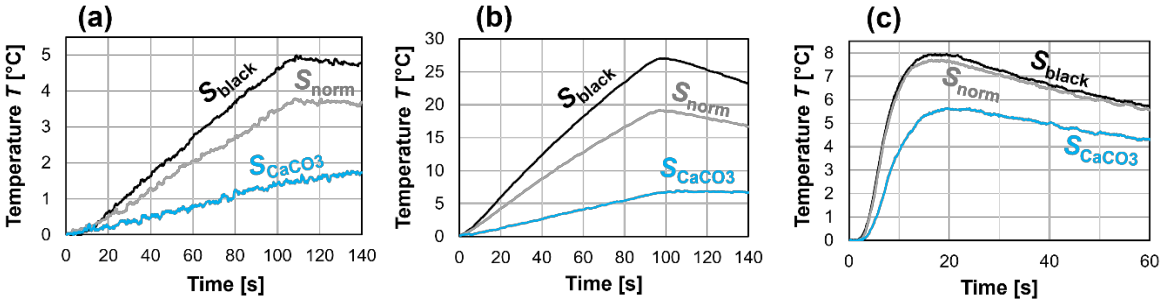

Fig. 4 Experimentally observed temperature increases for three specimens when using (a) visible light (< 900 nm), (b) short wavelength light (850–1600 nm), and (c) CO_2 laser (10600 nm).

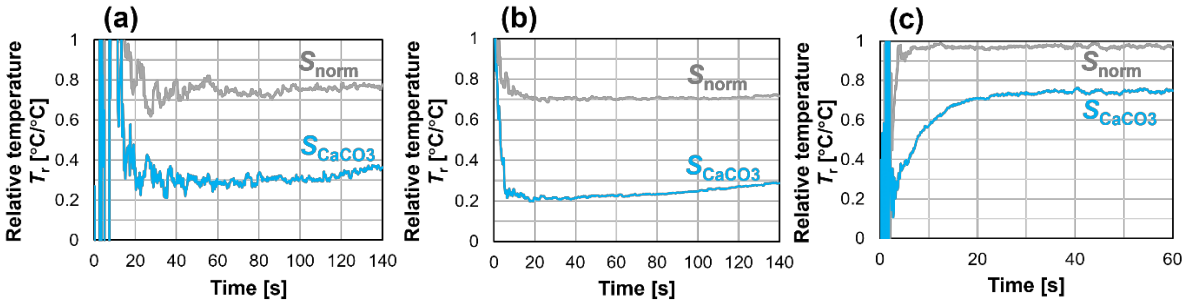

Fig. 5 Relative temperature increases T_r obtained by normalizing temperatures (in Fig. 4) of S_{norm} and S_{CaCO3} by that of S_{black} when using (a) visible light, (b) short wavelength light, and (c) CO_2 laser.

4. Inspection of mortar specimens with an artificial defect

The relationship between the heating efficiency and the surface spectral absorptivity, which depends on the wavelength of the heating light, was investigated in the previous section. Meanwhile, the inspection capability of active thermography depends on the heating efficiency. Thus, the inspection capability should also depend on the wavelength of the heating light. In this section, the inspections of specimens with artificial defects were performed using heating lights with different wavelengths, and the defect detection capabilities were compared.

4.1 Experimental setup

Figures 6 (a)–(c) show the photographs of the three mortar specimens and Fig. 6(d) shows a schematic of the specimens. The specimens were 85 mm × 100 mm × 55 mm and had an insertion of polystyrene foam with a thickness of 5 mm as an artificial defect (the polystyrene foam insertion was used to simulate an air gap in mortars because of its low density and thermal conductivity similar to those of air). The defect width and depth from the heated surface were 30 mm and 5 mm, respectively. The surface conditions of the specimens were the same as those shown in Fig. 1 (S_{norm}, S_{CaCO3}, and S_{black}). The specimens were heated using the same halogen lamp or CO_2 laser described in the previous section. Unlike the experiments in the previous section, the halogen lamp was equipped with no filters to input enough heat to the specimen; thus, the input light had wavelengths in both the visible and short wavelength ranges (the spectral absorptivity of visible and short wavelength light were similar, as shown in Fig. 2). In these experiments, the heater and infrared camera were placed on the same side, and the temperature of the heated surface was monitored using an infrared camera (i.e., single-side reflection inspection was performed because it is the most frequently used active thermography inspection method). In halogen lamp heating, the specimens were heated for 100 s and cooled in the air for 40 s; the surface temperatures were observed for total 140 s (both during heating and cooling). In contrast, when using the CO_2 laser, the heating and cooling duration were approximately 10 and 60 s, respectively; only the temperature during cooling was observed in order to protect the infrared detector from the scattered laser during heating. Thermal images were obtained using the same infrared camera used in Section 3 with a sampling frequency of 3.75 Hz. The distance between the infrared camera and the specimens was 300 mm. From the observed thermal images of each specimen, the temperature difference ΔT between the defective and non-defective areas was obtained, and the relative temperature difference ΔT_{r} of S_{norm} and S_{CaCO3} was obtained by normalizing the ΔT of S_{norm} and S_{CaCO3} by that of S_{black}. The ΔT_{r} values were also compared with

A_r presented in Fig. 2.

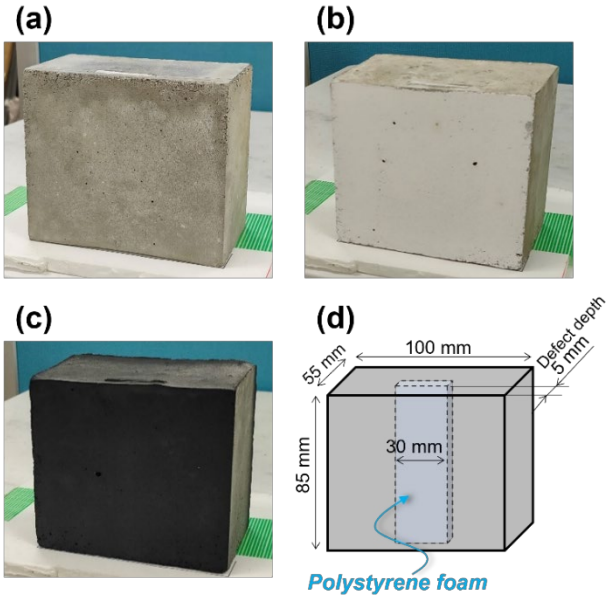

Fig. 6 Photographs of mortar specimens with an artificial defect (a) S_{norm}, (b) S_{CaCO3}, (c) S_{black}, and (d) schematic of the specimens.

4.2 Results

The thermal images observed when using the halogen lamp and the CO_2 laser are presented in Figs. 7 and 8, respectively. In each image, the defective area (surface above the polystyrene foam insertion) was detected as hotter than the non-defective area, and the temperature difference ΔT of S_{CaCO3} looks smaller than that of S_{norm} and S_{black}. The obtained ΔT and ΔT_r of the three specimens as a function of time are presented in Figs. 9 and 10, respectively. Figure 10 shows that ΔT_r obtained when using the CO_2 laser was larger than that obtained when the halogen lamp was used; when using the CO_2 laser, ΔT_r reaches approximately 100% for S_{norm} and was approximately 60% for S_{CaCO3}. The obtained ΔT_r values of S_{norm} and S_{CaCO3} (determined as the average of the values for 110–140 s and 40–70 s, respectively) are plotted as cross plots in Fig. 2. It should be noted that because the observed surface was the same as the heated surface in these experiments, the change in surface emissivity also affected the observation by the infrared camera [38–40]. From the results in Fig. 2, the average spectral absorptivity of S_{norm} and S_{CaCO3} in the wavelength range of 7.5–13μm, which is the detectable wavelength range of the camera used, is approximately 100% and 86%, respectively. Thus, for comparison with A_r in Fig. 2, when estimating the ΔT_r values of S_{CaCO3}, the results in Fig. 10 are multiplied by 100/86. By comparing the ΔT_r values with A_r in Fig. 2, it is found that the temperature difference observed in the defective area has a clear correlation with A_r. These results demonstrate that defects in mortars, including discolored mortars,

can be detected efficiently using light with wavelengths in the long wavelength range.

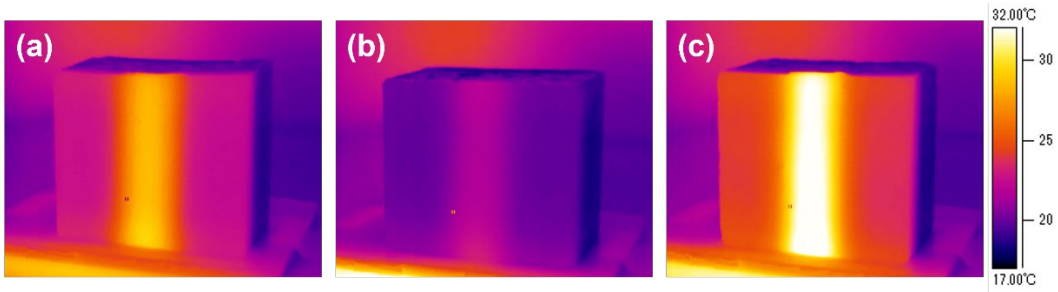

Fig. 7 Thermal images at 140 s obtained when using a halogen lamp for mortar specimen (a) S_{norm}, (b) S_{CaCO3}, and (c) S_{black}.

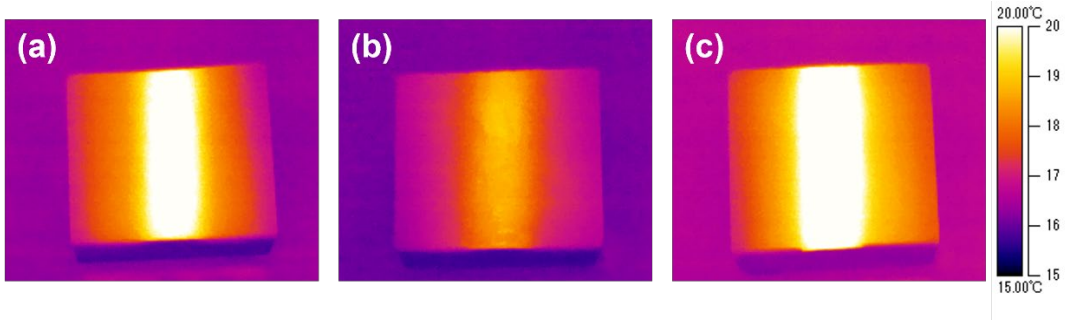

Fig. 8 Thermal images at 60 s obtained when using CO_2 laser for mortar specimen (a) S_{norm}, (b) S_{CaCO3}, and (c) S_{black}.

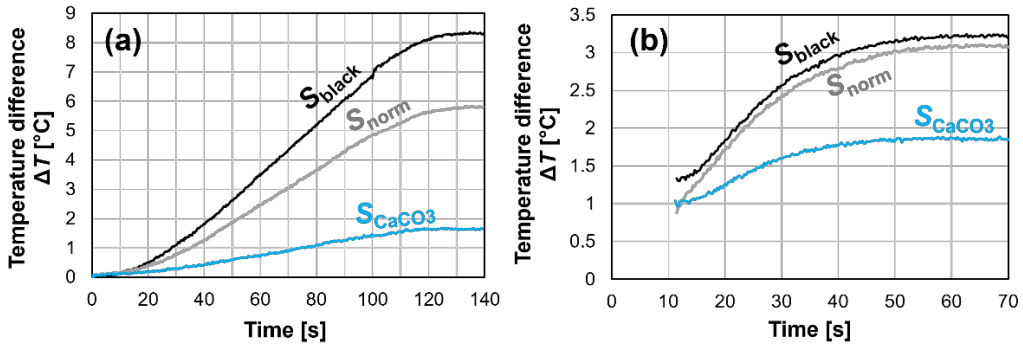

Fig. 9 Experimentally observed temperature difference ΔT between the defective and non-defective areas for three specimens when using (a) halogen lamp and (b) CO_2 laser.

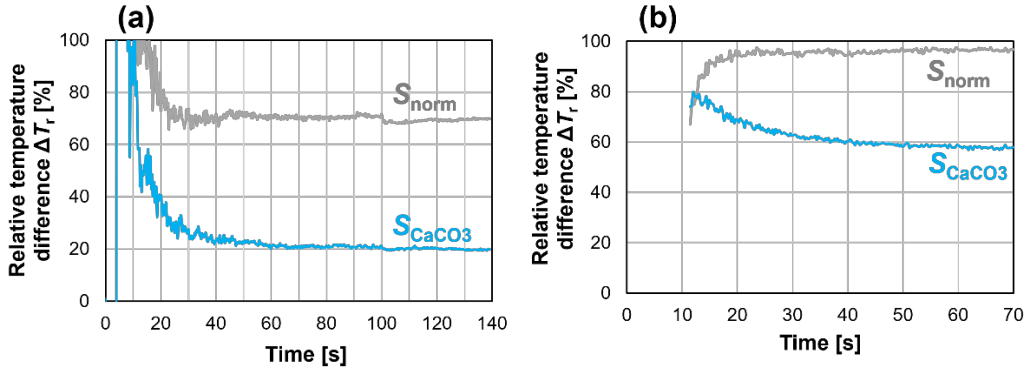

Fig. 10 Relative temperature difference ΔT_r obtained by normalizing ΔT of S_{norm} and S_{CaCO3} by that of S_{black} when using (a) halogen lamp and (b) CO_2 laser.

5. Conclusions

In this study, the surface spectral absorptivity of mortars discolored by the occurrence of $CaCO_3$ efflorescence was measured, and the effective heating light wavelengths for active thermography inspection of the discolored mortars was investigated. Spectroscopic measurements revealed that the surface spectral absorptivity of mortars significantly increased at a wavelength of approximately 3000 nm regardless of the presence/absence of the discoloration; the absorptivity in the long wavelength range was higher than that in the visible/short wavelength range. Experiments using optical light with three different wavelength ranges showed that the heating efficiency and defect detection capability (temperature difference observed in the defective region) correlate with the surface spectral absorptivity. The defects in the discolored specimen were detected more efficiently when using a CO_2 laser (light in the long wavelength range) than when using a halogen lamp (visible/short wavelength light). These results indicate that, although long wavelength light is conventionally known to be easily absorbed by concretes, it is also suitable for heating mortars whose surface is covered with calcium carbonate, and that using long wavelength light is an effective method for enhance the inspection capability of active thermography inspection of surface-whitened mortars.

Acknowledgements

The surface absorptivity of the specimens in the medium/long wavelength range was

measured at Tokyo Metropolitan Industrial Technology Research Institute.

Authors' contributions

Masashi Ishikawa conceptualized the study, conducted the experiments, and wrote the main manuscript text, Akira Emoto designed the experiments and interpreted the results, Yoshihiro Suto conducted experiments and prepared figures, and Hideo Nishino supervised and evaluated the results. All authors reviewed the manuscript.

Funding

No funding was received for conducting this study.

Availability of data and material

The datasets generated during and/or analyzed during the current study are available from the corresponding author on reasonable request.

Declarations

Ethics approval and consent to participate:

Not applicable.

Consent for publication:

Not applicable.

Competing interests:

The authors declare that they have no competing interests.

References

[1] Shepard SM (2007) Flash thermography of aerospace composites. In: IV Conferencia Panamericana de END Buenos Aires, Vol. 7, p. 26.

[2] Vavilov VP, Pawar, SS (2015) A novel approach for one-sided thermal nondestructive testing of composites by using infrared thermography. Polym Test 44:224–233.

https://doi.org/10.1016/j.polymertesting.2015.04.013.

[3] Wang F, Liu J, Dong B, Gong J, Peng W, Wang Y, Chen M, Liu G (2021) Blind image separation for the debonding defects recognition of the solid propellant rocket motor cladding layer using pulse thermography. Measurement 174:108997. https://doi.org/10.1016/j.measurement.2021.108997.

[4] D.'Accardi E, Palumbo D, Errico V, Fusco A, Angelastro A, Galietti U (2023) Analysing the Probability of Detection of Shallow Spherical Defects by Means of Pulsed Thermography. J Nondestruct Eval 42(1):27. https://doi.org/10.1007/s10921-023-00936-y.

[5] Sfarra S, Yao Y, Zhang H, Perilli S, Scozzafava M, Avdelidis NP, Maldague XPV (2019) Precious walls built in indoor environments inspected numerically and experimentally within long-wave infrared (LWIR) and radio regions. J Therm Anal Calorim 137:1083–1111. https://doi.org/10.1007/s10973-019-08005-1.

[6] Pan X, Xiang T, He Y, Wu J, Xia H, Lei T, Wang J (2023) A crack detection method for aero-engine blade based on air-flow thermography. J Nondestruct Eval, 42(1):22. https://doi.org/10.1007/s10921-023-00928-y.

[7] Ishikawa M, Ando M, Koyama M, Nishino H (2019) Active thermographic inspection of carbon fiber reinforced plastic laminates using laser scanning heating. Compos Struct 209:515–522. https://doi.org/10.1016/j.compstruct.2018.10.113.

[8] Archer T, Beauchêne P, Passilly B, Roche JM (2021) Use of laser spot thermography for the non-destructive imaging of thermal fatigue microcracking of a coated ceramic matrix composite. Quant InfraRed Thermogr J 18(3):141–158. https://doi.org/10.1080/17686733.2019.1705732.

[9] Roemer J, Khawaja H, Moatamedi M, Pieczonka L (2023) Data processing scheme for laser spot thermography applied for nondestructive testing of composite laminates. J Nondestruct Eval 42(1):21. https://doi.org/10.1007/s10921-023-00932-2.

[10] Favro LD, Han X, Ouyang Z, Sun G, Sui H, Thomas RL (2000) Infrared imaging of defects heated by a sonic pulse. Rev Sci Instrum 71(6):2418–2421. https://doi.org/10.1063/1.1150630.

[11] Morbidini M, Cawley P (2009) The detectability of cracks using sonic IR. J Appl Phys 105(9):093530. https://doi.org/10.1063/1.3125444.

[12] Guo X, Vavilov V (2013) Crack detection in aluminum parts by using ultrasound-excited infrared thermography. Infrared Phys Technol 61:149–156. https://doi.org/10.1016/j.infrared.2013.08.003.

[13] Pan M, He Y, Tian G, Chen D, Luo F (2012) Defect characterisation using pulsed eddy current thermography under transmission mode and NDT applications. NDT & E Int 52:28–36. https://doi.org/10.1016/j.ndteint.2012.08.007.

[14] He Y, Tian G, Pan M, Chen D (2014) Impact evaluation in carbon fiber reinforced plastic (CFRP) laminates using eddy current pulsed thermography. Compos Struct 109:1–7. https://doi.org/10.1016/j.compstruct.2013.10.049.

[15] He M, Zhang L, Zheng W, Feng Y (2017) Crack detection based on a moving mode of eddy current thermography method. Measurement 109:119–129. https://doi.org/10.1016/j.measurement.2017.05.041.

[16] Wiggenhauser H (2002) Active IR-applications in civil engineering. Infrared Phys Technol 43(3-5):233–238. https://doi.org/10.1016/S1350-4495(02)00145-7.

[17] Avdelidis NP, Moropoulou A (2004) Applications of infrared thermography for the investigation of historic structures. J Cultural Heritage 5(1):119–127. https://doi.org/10.1016/j.culher.2003.07.002.

[18] Maierhofer C, Arndt R, Röllig M, Rieck C, Walther A, Scheel H, Hillemeier B (2006) Application of impulse-thermography for non-destructive assessment of concrete structures. Cem Concr Compos 28(4):393–401. https://doi.org/10.1016/j.cemconcomp.2006.02.011.

[19] Kurita K, Oyado M, Tanaka H, Tottori S (2009) Active infrared thermographic inspection technique for elevated concrete structures using remote heating system. Infrared Phys Technol 52(5):208–213. https://doi.org/10.1016/j.infrared.2009.07.010.

[20] Schlichting J, Brauser S, Pepke LA, Maierhofer C, Rethmeier M, Kreutzbruck M (2012) Thermographic testing of spot welds. NDT & E Int 48:23–29. https://doi.org/10.1016/j.ndteint.2012.02.003.

[21] Broberg P (2013) Surface crack detection in welds using thermography. NDT & E Int 57:69–73. https://doi.org/10.1016/j.ndteint.2013.03.008.

[22] Sharp N, Adams D, Caruthers J, David A, Suchomel M (2014) Lithium-ion battery electrode inspection using pulse thermography. NDT & E Int 64:41–51. https://doi.org/10.1016/j.ndteint.2014.02.006.

[23] Doroshtnasir M, Worzewski T, Krankenhagen R, Röllig M (2016) On-site inspection of potential defects in wind turbine rotor blades with thermography. Wind energy 19(8):1407–1422. https://doi.org/10.1002/we.1927.

[24] Almond DP, Peng W (2001) Thermal imaging of composites. J Microsc 201(2):163–170. https://doi.org/10.1046/j.1365-2818.2001.00762.x.

[25] Avdelidis NP, Hawtin BC, Almond DP (2003) Transient thermography in the assessment of defects of aircraft composites. NDT & E Int 36(6):433–439. https://doi.org/10.1016/S0963-8695(03)00052-5.

[26] Maierhofer C, Myrach P, Reischel M, Steinfurth H, Röllig M, Kunert M (2014) Characterizing damage in CFRP structures using flash thermography in reflection and transmission configurations. Compos Part B: Eng 57:35–46. https://doi.org/10.1016/j.compositesb.2013.09.036.

[27] Vavilov V, Chulkov A, Dubinskii S, Burleigh D, Shpilnoi V, Derusova D, Zhvyrblia V (2021) Nondestructive testing of composite T-Joints by TNDT and other methods. Polym Test 94:107012. https://doi.org/10.1016/j.polymertesting.2020.107012.

[28] Carvalho MS, Martins AP, Santos TG (2019) Simulation and validation of thermography inspection for components produced by additive manufacturing. Appl Therm Eng 159:113872. https://doi.org/10.1016/j.applthermaleng.2019.113872.

[29] Silva H, Martins A, Machado MA, Santos TG, Carvalho MS (2023) Double active thermographic inspection of additive manufacturing composites: numerical modelling and validation. Measurement 218:113212. https://doi.org/10.1016/j.measurement.2023.113212.

[30] Dow C, Glasser FP (2003) Calcium carbonate efflorescence on Portland cement and building materials. Cem Concr Res 33(1):147–154. https://doi.org/10.1016/S0008-8846(02)00937-7.

[31] Brocken H, Nijland TG (2004) White efflorescence on brick masonry and concrete masonry blocks, with special emphasis on sulfate efflorescence on concrete blocks. Constr Build Mater 18(5):315–323. https://doi.org/10.1016/j.conbuildmat.2004.02.004.

[32] Ludwig N, Rosina E (2005) Dynamic IRT for the frescoes assessment: the study case of Danza Macabra in Clusone (Italy). Proc. SPIE 5782, Thermosense XXVII. https://doi.org/10.1117/12.604648

[33] Ishikawa M, Tsukagoshi M, Kasano H, Nishino H (2021) Influence of composition and surface discoloration of concrete on active thermographic nondestructive inspection. Measurement 168:108395. https://doi.org/10.1016/j.measurement.2020.108395.

[34] FLIR (2011) User's manual FLIR A3xx series.

[35] de LÉclarage Commision Internationale (2004) CIE 15: 2004 Technical Report Colorimetry

[36] Shimadzu Corporation, The Structure of a Spectrophotometer. Shimadzu Corporation website. https://www.shimadzu.com/an/service-support/technical-support/analysis-basics/fundamentals-uv/structure.html. Accessed 18 October 2023.

[37] Parker WJ, Jenkins RJ, Butler CP, Abbott GL (1961) Flash method of determining thermal

diffusivity, heat capacity, and thermal conductivity. J Appl Phys 32(9):1679–1684. https://doi.org/10.1063/1.1728417.

[38] Avdelidis NP, Moropoulou A (2003) Emissivity considerations in building thermography. Energ Build 35(7):663–667. https://doi.org/10.1016/S0378-7788(02)00210-4.

[39] Barreira E, de Freitas VP (2007) Evaluation of building materials using infrared thermography. Constr Build Mater 20(1):218–224. https://doi.org/10.1016/j.conbuildmat.2005.06.049.

[40] Marinetti S, Cesaratto PG (2012) Emissivity estimation for accurate quantitative thermography. NDT & E Int 51:127–134. https://doi.org/10.1016/j.ndteint.2012.06.001.